International Journal of Mass Spectrometry 308 (2011) 209–216

Contents lists available at ScienceDirect

International Journal of Mass Spectrometry

journal homepage: www.elsevier.com/locate/ijms

Tyrosine nitration as evidenced by IRMPD spectroscopy

Rajeev K. Sinha[a,1], Barbara Chiavarino[a], Maria Elisa Crestoni[a], Debora Scuderi[b], Simonetta Fornarini[a,*]

[a] Dipartimento di Chimica e Tecnologie del Farmaco, Università di Roma "La Sapienza", P.le A. Moro 5, 00185 Roma, Italy
[b] Laboratoire de Chimie Physique, UMR8000 Université Paris-Sud 11, Faculté des Sciences d' Orsay, Batiment 350, 91405 Orsay Cedex, France

ARTICLE INFO

Article history:
Received 9 May 2011
Received in revised form 1 July 2011
Accepted 11 July 2011
Available online 20 July 2011

Dedicated to Professor John R. Eyler in admiration for his contributions to gas-phase ion chemistry and FT-ICR mass spectrometry and in appreciation for his scientific mentoring.

Keywords:
Amino acid
Protein modification
Vibrational spectroscopy
Electrospray ionization mass spectrometry
Ab initio calculations

ABSTRACT

Protonated 3-nitrotyrosine ([nitroTyr + H]$^+$) has been investigated by collision induced dissociation at variable energy and by IR multiple photon dissociation (IRMPD) spectroscopy in conjunction with quantum chemical calculations. Ultimately, this investigation is aimed at providing a diagnostic signature of protein tyrosine nitration, a post translational modification implied in pathological states. IRMPD spectroscopy of [nitroTyr + H]$^+$ ions has been examined in two different spectral regions, namely in the 1000–2000 cm^{-1} range, using the free electron laser beamline at the CLIO facility, and in the 3200–3700 cm^{-1} range, using a tabletop laser source. [nitroTyr + H]$^+$ ions have been assayed in parallel with intact [Tyr + H]$^+$ ions revealing characteristic bands at 1329 and 1540 cm^{-1}. Mode assignments allowed by density functional theory calculations of the IR spectra of the most stable conformers indicate that these features are associated to vibrations of the nitro group and are endowed with enhanced activity. In the NH/OH stretching region, the remarkable difference between the IRMPD spectra is the strong absorption at 3641 cm^{-1} of the ring OH stretching of [Tyr + H]$^+$ which is absent in the nitrated ion due to a strong hydrogen bond engaging the ring OH and the ortho nitro group. These results suggest that IRMPD spectroscopy and tandem mass spectrometry may afford a selective method for the analysis and characterization of 3-nitrotyrosine, to be possibly extended to 3-nitrotyrosine-containing peptides.

1. Introduction

The nitration of protein tyrosine residues is considered as one of the molecular footprints revealing the action of reactive oxygen and nitrogen radical species, that are often implicated in the pathogenesis of a number of diseases [1–4]. Tyrosine is modified in the 3-position of the phenolic ring, leading to a 3-nitro-derivative which may impair the protein structure and function. Different free radical pathways may account for biological protein tyrosine nitration and are indicated to involve excess NO, oxidants and metal centers.

Also in consideration of the biomarker function of protein tyrosine nitration, a variety of analytical methods have been devised to allow the detection and quantification of 3-nitrotyrosyne [5–7]. Approaches based on mass spectrometry have provided structural information and permitted the quantification of trace quantities. One may cite the identification of a protein nitration site that has been obtained using electrospray ionization (ESI) coupled to FT-ICR mass spectrometry to analyze the protein digestion mixture [8,9]. In some instances, though, mass spectrometric methods face difficulties related to artifactual formation of nitrated tyrosine during sample treatment and photodecomposition processes affecting the nitro group in MALDI analysis [7,10,11]. For example MALDI laser light at 337 nm, widely used for the analysis of peptides and proteins, activates decomposition processes explained by the vicinity (at ca. 230 nm) of the absorbance maximum of nitrotyrosine under acidic conditions [12]. These photofragmentation reactions are thus a characteristic of nitrated peptides, however their occurrence is a drawback if one strives to obtain clear evidence for a molecular ion of the nitrated peptide in a complex peptide pattern [13–16].

In another perspective, the activation of a photofragmentation process can be exploited to perform an IR spectroscopic assay in order to gain diagnostic information about 3-nitrotyrosine that may potentially reveal the presence of this biomarker. This is a challenging task, though, given the very low abundance of protein tyrosine nitration in vivo [1].

The present work is aimed at obtaining a comprehensive pattern of the IR absorption features of 3-nitrotyrosine, ionized in an electrospray ion source by the addition of a proton. The so-obtained protonated species ([nitroTyr + H]$^+$) has been examined in an isolated state, submitting it to IR multiple photon dissociation (IRMPD) spectroscopy. The purpose was to ascertain individual features characterizing protonated 3-nitrotyrosine, that may aid the mass spectrometric detection of this post translational

* Corresponding author. Tel.: +39 06 4991 3510; fax: +39 06 4991 3602.
E-mail address: Simonetta.fornarini@uniroma1.it (S. Fornarini).
[1] Present address: Department of Chemistry and Biochemistry, University of Bern, Freistrasse 3, CH-3012 Bern, Switzerland.

1387-3806/$ – see front matter © 2011 Elsevier B.V. All rights reserved.
doi:10.1016/j.ijms.2011.07.012

modification. IRMPD spectroscopy of gaseous ions is a rapidly growing field that has been producing an impressive amount of valuable information on the building elements of peptides and proteins in recent years, as described in a recent review article by John Eyler who has himself given paramount spur and contribution to the field [17–21]. The natural amino acids are benchmark species investigated by IRMPD spectroscopy under various ionic forms derived from the attachment of a proton or a metal ion. Among the structural questions that were addressed, the amino acid–alkali metal cation complexes have been identified as either salt bridge (zwitterion) or charge solvated isomers, in each case presenting the features corresponding to the lowest energy species [22–31].

In the present work, the $[nitroTyr + H]^+$ ion has been assayed by IRMPD spectroscopy in two spectral regions taking advantage of two different instrumental platforms. The IR 'fingerprint' region in the 1000–2000 cm^{-1} range was accessed using a 7T FT-ICR (Fourier Transform Ion Cyclotron Resonance) mass spectrometer coupled with the IR beamline of the free electron laser (FEL) at the CLIO (Centre Laser InfraRouge d'Orsay) facility. Systems combining IR-FEL radiation with FT-ICR mass spectrometry have proven highly fruitful in yielding IR spectroscopic characterization of a variety of gaseous ions [32–34]. The 3200–3700 cm^{-1} region was explored using an apparatus assembled at the Università di Roma "La Sapienza" where a commercial Paul-type ion trap was modified to admit the IR radiation of an optical parametric oscillator/amplifier (OPO/OPA) laser source [35], as already described in a similar setup [36].

It should be finally mentioned that the consequences of a post translational modification in amino acids and peptides have already been investigated by IRMPD spectroscopy in the case of the phosphorylation of an OH functionality in the side chain of serine, threonine and tyrosine and two representative peptides [36–38]. The P═O stretching band, active in the 1200–1300 cm^{-1} region, was found to be very sensitive to the surrounding environment. Falling in a region of relatively low IR activity for peptides, it fulfills the prerequisites to provide an analytical tool for phosphorylated sites. The oxidation of methionine has also been recently revealed by IRMPD spectroscopy by the associated S═O bond signature [39]. Along a similar line of investigation, a special focus will be placed on the characteristic modes possibly revealing the presence of the nitro group in 3-nitrotyrosine. For comparison purposes, protonated tyrosine has been examined as well.

2. Experimental details

All reagents were commercial products (Sigma–Aldrich s.r.l. Milan, Italy) and were used as received. Protonated tyrosine and nitrotyrosine ions ($[Tyr + H]^+$, m/z 182, and $[nitroTyr + H]^+$, m/z 227), are formed by electrospray ionization (ESI) by directly infusing a 5 μM methanol/water (50/50 with 1% acetic acid) solution of the amino acid through a fused-silica capillary to the ESI source by a syringe pump at a typical flow rate of 2 μL min^{-1}.

Mass spectrometric experiments of energy-variable collisionally activated dissociation were carried out using a 2000 Q TRAP instrument (Applied Biosystems), a commercial hybrid triple quadrupole linear ion trap mass spectrometer ($Q1q2Q_{LIT}$). The ion of interest was mass-selected using Q1. Collision induced dissociation (CID) experiments were performed in the quadrupole collision cell q2 at variable collision energies (E_{lab} = 5–50 eV). The nominal pressure of the N_2 collision gas was typically set at 2.4–4.0 × 10^{-5} mbar. The ionic products were monitored by scanning Q_{LIT}.

The IRMPD spectra of the mass-selected ions were recorded employing two different experimental setups. The mid-infrared region (1000–2200 cm^{-1}) was explored using the tunable IR radiation of the FEL beamline at CLIO coupled to a modified commercial 7 T Fourier transform ion cyclotron resonance (FT-ICR) mass spectrometer (Bruker, Apex Qe) [32]. The ions of interest, generated by an Apollo II ESI source as described above, were mass-selected in the quadrupole mass filter, and collisionally cooled with argon (removing any excess kinetic energy) in a hexapole cell. The ions were then pulsed into the FT-ICR cell where they were trapped at a background pressure of about 1.5 × 10^{-9} mbar and exposed to IR light for a fixed time. At each wavelength, the mass-spectrum is the Fourier transform of the average of five time-domain transients. The 25 Hz FEL radiation delivers typical macropulse energies of 40 mJ. Ions were irradiated with 4–10 macropulses. For the present study, the FEL was operated at 45 MeV in order to optimize the laser power in the frequency region of interest. The laser wavelength profile was monitored at each reading with a monochromator associated with a pyroelectric detector array (spiricon). The laser power displayed a smooth variation around a fairly constant value throughout the wavelength range explored, going from 720 mW at 1000 cm^{-1} to 900 mW in the range between 1100 and 1700 cm^{-1} and down to 745 at 1830 cm^{-1}.

The 3200–3700 cm^{-1} spectral range was investigated using an apparatus whereby the radiation output of a tabletop IR optical parametric oscillator/amplifier (OPO/OPA; Laser Vision) is admitted into a modified Bruker Esquire 6000+ ion-trap mass spectrometer. The parametric converter is pumped by an Nd:YAG laser (Continuum Surlite II) operating at 10 Hz repetition rate and delivering 600 mJ/pulse (4–6 ns long). In the investigated spectral range, the typical output pulse energy from the OPO/OPA laser source was 28 mJ/pulse, with a spectral bandwidth of about 3–4 cm^{-1}. In the ion trap $[nitroTyr + H]^+$ ions were mass-selected and accumulated for 20 ms prior to IR irradiation. IRMPD spectroscopy of the mass-selected and accumulated ions was performed using the MS2 step, keeping the excitation amplitude zero to avoid any collision induced fragmentation. Post irradiation mass spectra were recorded after 6 accumulations. The irradiation time is controlled using an electromechanical shutter synchronized with the mass spectrometer. The typical irradiation time used in the experiment is 1 s.

Monitoring the abundances of the fragment ions relative to the parent ion abundance reveals the occurrence of the photofragmentation process at the IR active wavelengths. The IRMPD spectrum is plotted by recording the photofragmentation yield R ($R = -\ln[I_{parent}/(I_{parent} + \Sigma I_{fragments})]$ where I_{parent} and $I_{fragments}$ are the integrated intensities of the mass peaks of the precursor and of the fragment ions, respectively) as a function of the photon energy [40,41]. Care was taken to keep the photofragmentation yield low ($\Sigma I_{fragments} \leq 0.5\, I_{parent}$) in order to minimize saturation effects and prevent secondary photofragmentation events.

A computational survey was made selecting the most stable conformers for protonated nitrotyrosine and performing harmonic frequency analysis on the optimized geometries. All calculations were performed using the Gaussian 03 or Spartan 08 software packages. A conformational search was run first, using the MMFF molecular mechanics model. Out of 10,000 conformers examined, the lowest energy 30 structures were kept and used as starting geometries for hybrid DFT calculations at progressively increasing levels of theory. While there is no guarantee that the global minimum will actually be identified, we note that a good agreement is found with the stable conformers of the protonated tyrosine derivatives previously reported [42–45]. Ultimately, geometries and harmonic vibrational frequencies were obtained at B3LYP/6-311++G** level. Enthalpies at 298 K were calculated using ZPE and thermal corrections obtained from unscaled harmonic frequencies. In order to obtain IR spectra for the species of interest to be compared with the experimental IRMPD spectra, the calculated

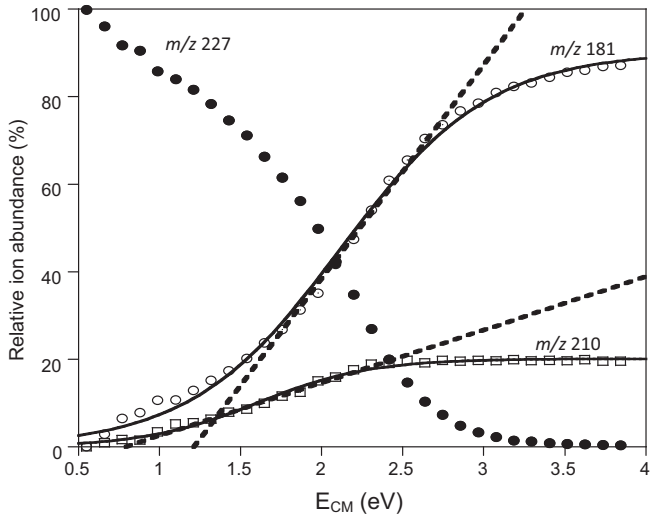

Fig. 1. Relative abundances of the parent ion (*m*/*z* 227) and daughter ions (*m*/*z* 210 and 181) as a function of collision energy (center of mass) upon CID of mass-selected [nitroTyr + H]$^+$ ions. The lines represent fits of the ion abundances using a sigmoid function. It should be noted that at higher collision energy other fragment ions appear, resulting from further fragmentation of ions at *m*/*z* 210 (yielding ions at *m*/*z* 168) and of ions at *m*/*z* 181 (yielding *m*/*z* 136, 117, and 90). Their abundances are summed to the ones of their precursors to give the profiles in the graph.

harmonic vibrational frequencies were scaled by a factor of 0.975 in the 1000–2000 cm^{-1} region and 0.955 in the 3200–3700 cm^{-1} frequency range. In the figures comparing the experimental IRMPD spectra with the computed ones, the calculated absorption lines are convoluted with a Lorentzian profile of 20 cm^{-1} fwhm (full width at half maximum) in the 1000–2000 cm^{-1} region while a fwhm of 10 cm^{-1} was used for the 3200–3700 cm^{-1} frequency range. MP2 calculations have been tested as well. They did not yield better agreement between calculated IR and experimental IRMPD spectra though.

3. Results and discussion

3.1. Photodissociation and CID mass spectra

When [nitroTyr + H]$^+$ ions at *m*/*z* 227 are mass-selected and irradiated at a photon energy in resonance with an IR active mode, fragment ions are observed at *m*/*z* 210 (corresponding to loss of NH_3) and at *m*/*z* 181 (corresponding to formal losses of H_2O and CO). The competitive losses of NH_3 and of H_2O + CO are typical of protonated aromatic amino acids under CID conditions, at variance with the preferential formation of benzyl-type cations via electron-induced dissociation processes [46–48]. The loss of H_2O + CO is also observed as a major channel in laser-induced dissociation of protonated tyrosine, as already reported [49,50]. Interestingly, these two fragmentation channels do not affect the nitro group, so that the amino acid modification is still retained in the fragment ion. Fig. 1S (Supplementary data) shows the photodissociation mass spectrum recorded upon irradiation at 1171 cm^{-1}, reflecting the mild activation of ions to the lowest energy fragmentation paths. This notion is supported by the breakdown curves reported in Fig. 1. The plots in this figure illustrate the relative abundances of parent and fragment ions when the parent ion at *m*/*z* 227 is selected in the first quadrupole of the Q TRAP instrument and is submitted to collision with N_2 target gas in the second quadrupole collision cell. The collision energy is reported in the center of mass frame. At onset dissociation energy the CID fragments are at *m*/*z* 210 and 181 in a relative ratio reflecting their yield in the IRMPD experiment. Fig. 2S shows that the ratio of their relative abundances

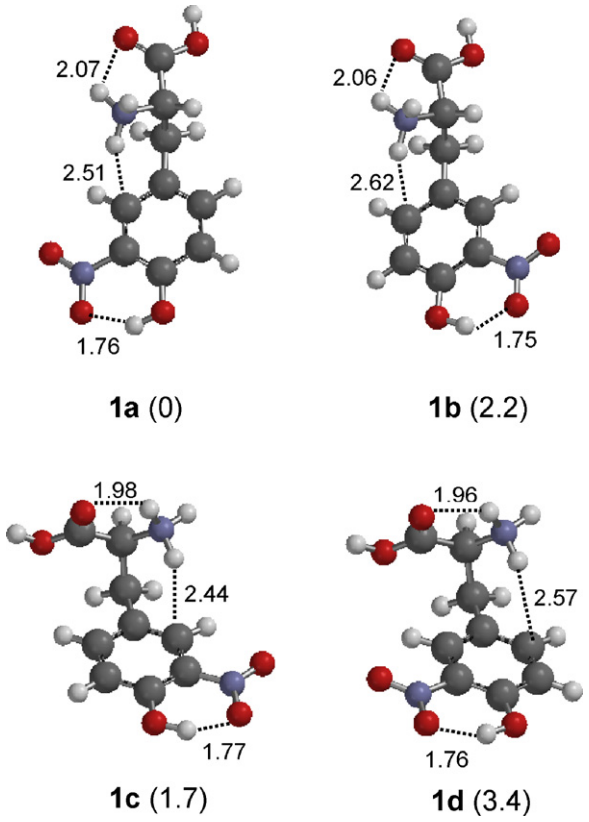

Fig. 2. Most stable conformers of protonated 3-nitrotyrosine [nitroTyr + H]$^+$, and relative energies at 298 K (kJ mol^{-1}) calculated at B3LYP/6-311++G** level of theory.

is constant throughout several IR active modes sampled in the 1000–2000 cm^{-1} region, which suggests that the ion assayed by IRMPD is either a unique species or a mixture of closely related structures.

3.2. Computed structures

The protonation of the common amino acids has been the subject of recent computational studies [42–45,51] and the protonation chemistry in the gas phase has been reviewed [52]. In tyrosine the relatively large loss of entropy upon protonation has been ascribed to the increased strength of the interaction between the amino hydrogens and the phenyl group in the protonated species and to the larger entropy of mixing associated with the population of the neutral conformers relative to the one of the protonated species [43]. Also the protonated nitrotyrosine ion [nitroTyr + H]$^+$, bears the additional proton on the amino group. The most stable conformers have been identified along the procedure outlined in Section 2. The four most stable geometries obtained by calculations at B3LYP/6-311++G** level are depicted in Fig. 2 and the relevant thermodynamic data, including the relative enthalpies of the protonated species at 298 K, are summarized in Table 1S. The rotation of 180° around the C(phenyl)-C bond does not affect the conformer relative energy to any appreciable extent (e.g., the energies of **1a** and **1b** differ by 2.2 kJ mol^{-1} and the energies of **1c** and **1d** differ by only 1.7 kJ mol^{-1}) and also the calculated IR spectra (vide infra) of the two pairs of species are quite similar. In other words, the orientation of the OH and the position of the NO_2 ring substituents relative to the side chain does not appear too influential. In these four most stable structures a cation-π interaction can be envisioned between the periphery of the aryl ring and a proton on the protonated amino group, as observed previously [53,54]. This interaction stabilizes the conformations of protonated tyrosine that

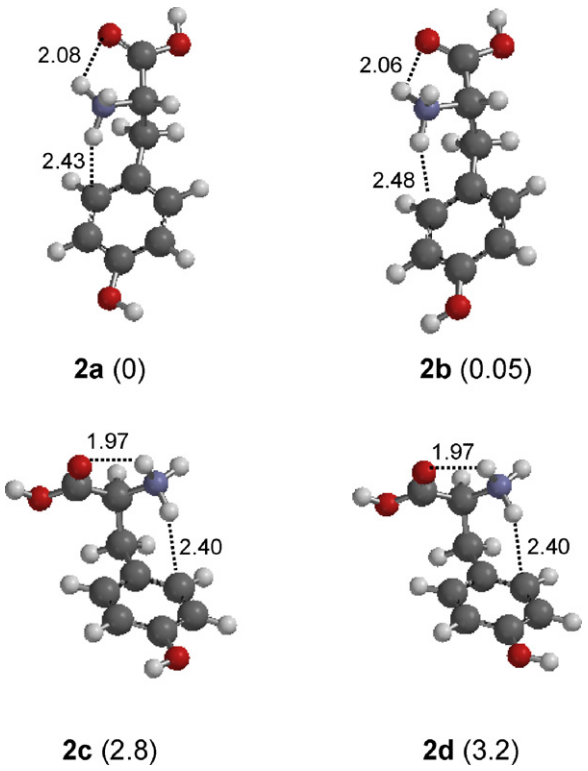

Fig. 3. Most stable conformers of protonated tyrosine $[Tyr+H]^+$, and relative energies at 298 K (kJ mol^{-1}) calculated at B3LYP/6-311++G** level of theory.

present this unconventional H-bond between the π system and the ammonium group by more than 15 kJ mol^{-1} [49]. Other characteristic features are the hydrogen bond between the ring-OH and the nitro group, a hydrogen bond between the amino group and the carbonyl oxygen and the syn geometry at the C(O)OH group. Other conformers are higher in energy. The next one in the energy ladder at 14.9 kJ mol^{-1} is depicted in Fig. 3S(**1e**). It is similar to **1c**, differing for the rotation of the carboxyl group which is oriented so to allow hydrogen bonding between a proton on the ammonio group and the hydroxylic oxygen atom. The rotational barriers associated to the interconversion between conformers (1a-1d) are on the order of 15 kJ mol^{-1} (see Figs. 4S and 5S in the Supplementary data), which should ensure fast equilibration at room temperature.

Other conceivable isomers of protonated nitrotyrosine have been explored as well. When the proton is placed on the carbonyl oxygen and a hydrogen bond is allowed with the N atom of the amino group, the geometry optimization moves the proton toward nitrogen to form an ammonium group. With a different orientation of the $[-C(OH)_2]^+$ group, a stable structure (**1x**, depicted in Fig. 3S) is found, lying at 105 kJ mol^{-1} relative to **1a**. Although the presence of the nitro group will render the aryl ring less basic than in native tyrosine, two conceivable ring-protonated isomers have been submitted to geometry optimization yielding **1y** and **1z** (at 52 and 143 kJ mol^{-1} relative energy). The relative stability of **1y** owes its origin from the covalent character of the bond between N and the C atom in para position with respect to the protonated one. The so-formed structure appears as a cyclohexadiene unit with a positively charged ammonium nitrogen. However, the high energy of these isomers does not support any relevant role in the sampled ion population.

A similar computational analysis has been performed on protonated tyrosine, yielding the four most stable conformers illustrated in Fig. 3. The geometry of these species (**2a–d**) is strictly comparable to the one of the corresponding protonated nitrotyrosine ions (**1b**, **1a**, **1d**, **1c**, respectively) if allowance is made for the additional

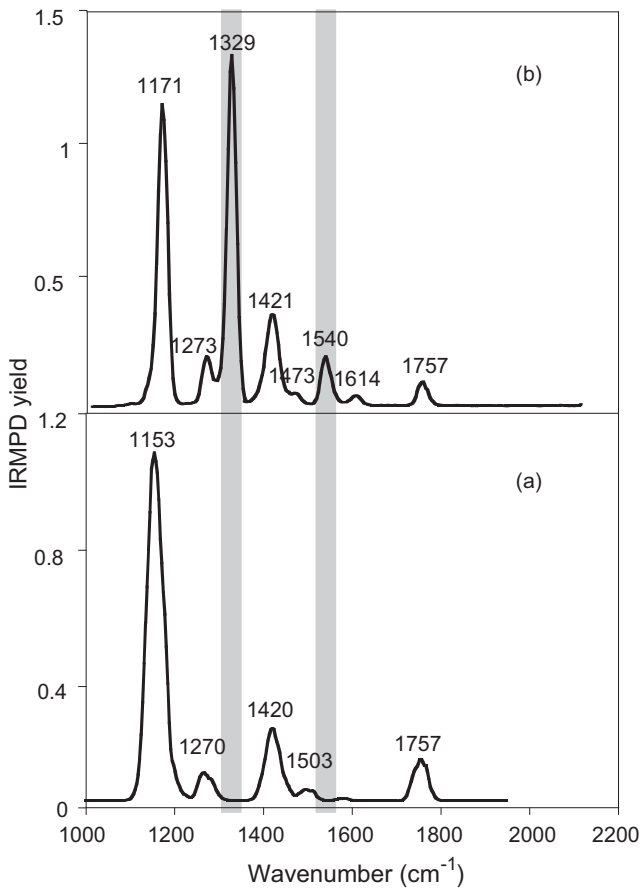

Fig. 4. IRMPD spectrum of $[Tyr+H]^+$ (a) and of $[nitroTyr+H]^+$ (b). The grey bars underline the position of characteristic bands in the IRMPD spectrum of $[nitroTyr+H]^+$.

presence of the nitro group in **1a–d**. As already noted [49], the protons on the $-NH_3^+$ group are engaged in bonding both with the π system and with the carbonyl oxygen. The four conformers lie all within 3.2 kJ mol^{-1} while the next more stable ones are separated by more than 15 kJ mol^{-1} with respect to **2a**.

Hydrogen bonds are marked by dashed lines in Figs. 2 and 3 and distances are given in Å.

3.3. IRMPD spectroscopy of protonated 3-nitrotyrosine (and of protonated tyrosine)

3.3.1. IRMPD spectra in the 1000–2000 cm^{-1} range

The IRMPD spectrum of $[nitroTyr+H]^+$ ions in the 1000–2000 cm^{-1} range is plotted in the upper panel of Fig. 4 together with the recorded spectrum of protonated tyrosine ($[Tyr+H]^+$, in the lower panel) to our knowledge not yet reported elsewhere. The general appearance of the IRMPD spectrum of $[nitroTyr+H]^+$ shows only modest congestion and broadening of the bands (for example the band at 1329 cm^{-1} is characterized by a full width at half maximum, fwhm, of ca. 22 cm^{-1}) which suggests either the presence of a single conformer or a mixture of conformers with very similar IR spectra. Indeed, the relative enthalpies of the most stable conformers indicate that these species should be present in comparable abundances in a Maxwell–Boltzmann averaged population. At the same time the similar structural features and bonding interactions are not likely to account for any meaningful differentiation by IRMPD spectroscopy. The spectrum of $[Tyr+H]^+$ (Fig. 4a) is dominated by a strong feature at 1153 cm^{-1} and other bands appear at 1270, 1420,

Table 1
IRMPD spectral frequencies of protonated tyrosine [Tyr+H]$^+$, and calculated (B3LYP/6-311++G**) vibrational frequencies of conformer **2a**.

Experimental IRMPD[a]	Calculated IR[a,b]	Vibrational mode
	1086 (75)	C–H and N–H bend
1153	1158 (329)	C–O stretch and COH bend of C(O)OH
	1162 (114)	C–H and COH bend of aryl group, ring def
1270	1276 (156)	C–OH ring stretch, ring def
	1392 (105)	CCO stretch of side chain and CH bend of side chain methine
1420	1438 (188)	NH_3 umbrella
1503	1506 (102)	C=C stretch, aromatic CH bend
	1608 (91)	C=C stretch
1757	1762 (293)	C=O stretch
	3120 (127)	symm NH_2 stretch (H's bound to CO and to aromatic system)
	3178 (346)	asymm NH_2 stretch (H's bound to CO and to aromatic system)
3334	3325 (109)	NH stretch (free)
3551	3552 (197)	OH stretch of C(O)OH
3641	3648 (128)	OH stretch (ring)

[a] In cm^{-1}.
[b] Only major bands (intensity greater than 50 km mol^{-1}, reported in parentheses) are listed.

1503, and 1757 cm^{-1}. Relying on the typically good agreement between the IRMPD spectrum and the linear IR spectrum of the sampled species obtained by hybrid DFT calculations [20], the vibrational modes of [Tyr+H]$^+$ can be assigned as described in Table 1. The experimental IRMPD features are listed together with the IR bands calculated for the most stable conformer **2a**, used as a basis to interpret the experimental IRMPD bands and the underlying vibrational modes. The matching of the IRMPD spectrum with the IR spectrum of conformer **2a** is illustrated in Fig. 5. It is conceivable that the sampled [Tyr+H]$^+$ ions comprise a thermally averaged population of the stable conformers **2a–d**, all lying within 3.2 kJ mol^{-1}. However, the individual IR spectra of conformers **2b–d** do not present significant differences with respect to conformer **2a** in the 1000–2000 cm^{-1} region, as shown in Fig. 6S (Supplementary Data), and will not be further considered.

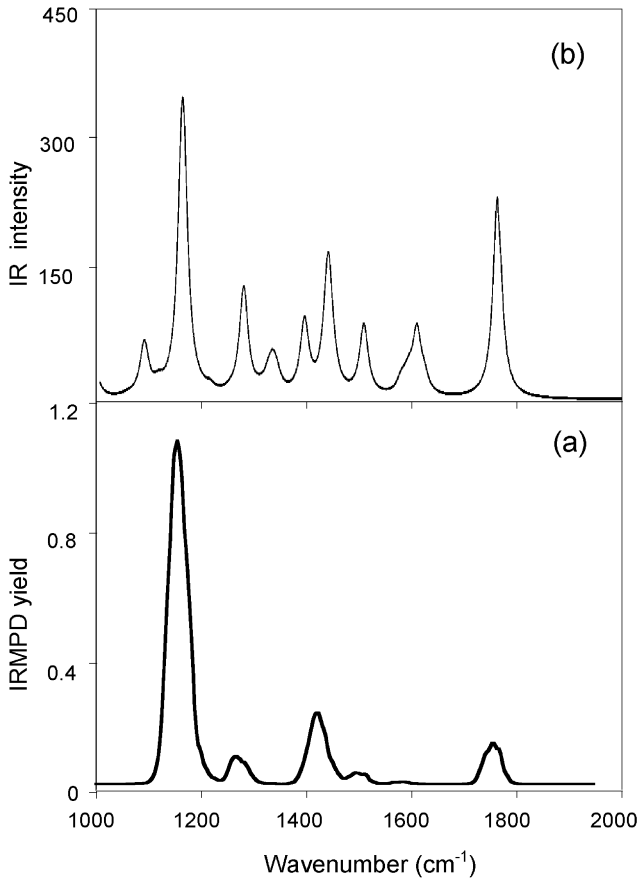

Fig. 5. IRMPD spectrum of [Tyr+H]$^+$ (a) and calculated IR spectrum of conformer **2a** of [Tyr+H]$^+$ (b) in the spectral range of 1000–2000 cm^{-1}.

The IRMPD spectrum of [nitroTyr+H]$^+$ (Fig. 4b) compared to the one of [Tyr+H]$^+$ (Fig. 4a) presents quite similar features with a pronounced band at 1171 cm^{-1} and weaker ones at 1273, 1421, 1614, and 1757 cm^{-1}. However, a second strong band appears at 1329 cm^{-1}: This band is missing in the IRMPD spectrum of [Tyr+H]$^+$. Similarly, the distinct feature at 1540 does not appear to have a corresponding one in the case of [Tyr+H]$^+$. The IRMPD spectrum of [nitroTyr+H]$^+$ may again be interpreted considering the calculated IR spectrum of the most stable conformer **1a**, as illustrated in Fig. 6 and by the data listed in Table 2. The calculated IR spectra of conformers **1b–d** do not differ to a significant extent from the IR spectrum of **1a** (see Fig. 7S in the Supplementary Data), therefore only the spectrum of conformer **1a** will be used as the basis for assigning the vibrational modes. One may note that the characteristic, strong feature at 1329 cm^{-1} is to be likely associated with the computed mode at 1347 cm^{-1}. This mode combines CH bending and in plane bending of the ring OH group with symmetric NO_2 stretching. We tentatively ascribe the enhanced activity of this vibration to the contribution of the polar NO_2 group imparting a notable oscillator strength. The NO_2 group is also involved in another band appearing with enhanced intensity in the IRMPD spectrum of [nitroTyr+H]$^+$, the one at 1540 cm^{-1}. This mode is associated with aromatic C=C stretching and asymmetric NO_2 stretching, once again involving the polar nitro group. It may then be concluded that two distinct IRMPD features showing exceptional activity are due to the presence of the nitro substituent and may be considered diagnostic of the modified aryl group of tyrosine.

One critical point that may be noticed in both Figs. 5 and 6, comparing the experimental IRMPD spectra with the calculated IR spectra, is that some weak bands have escaped observation despite the excellent S/N ratio. This is not an unusual finding, though [20,55–57]. Possible reasons have been ascribed to predicted intensities that are too high, to rates of photon absorption that are not adequate to promote the IRMPD process, to intramolecular vibrational relaxation processes that are not efficient.

3.3.2. IRMPD spectra in the 3200–3700 cm^{-1} range

The assay of [nitroTyr+H]$^+$ ions has been conducted also in the region from 3200 to 3700 cm^{-1}. The upper panel of Fig. 7 shows the IRMPD spectrum of [nitroTyr+H]$^+$ to be compared with the corresponding spectrum of [Tyr+H]$^+$ plotted in the lower panel. The IR spectra of conformers **1a–d** in the 3000–3700 cm^{-1} range

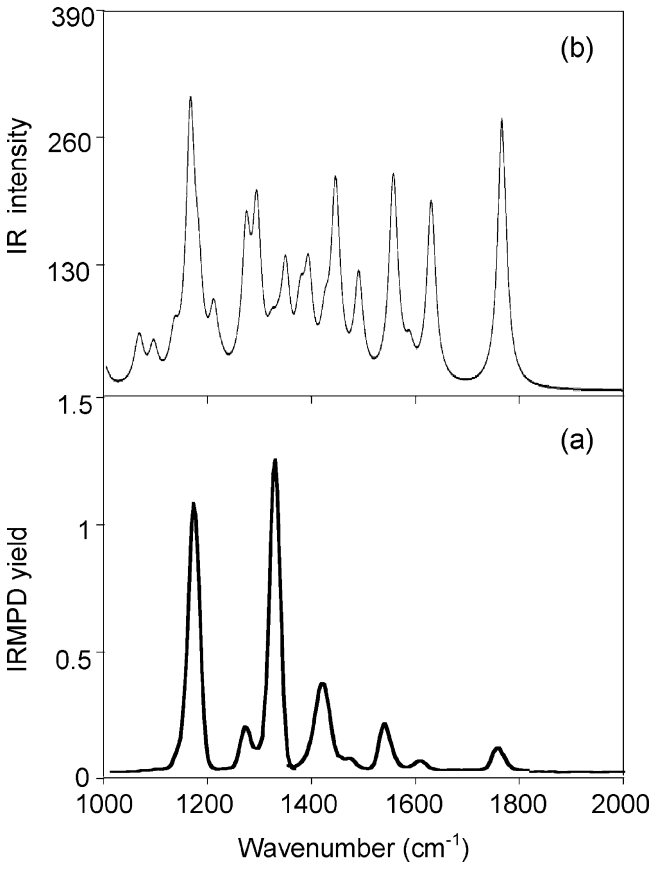

Fig. 6. IRMPD spectrum of $[nitroTyr+H]^+$ (a) and calculated IR spectrum of conformer **1a** of $[nitroTyr+H]^+$ (b) in the spectral range of 1000–2000 cm^{-1}.

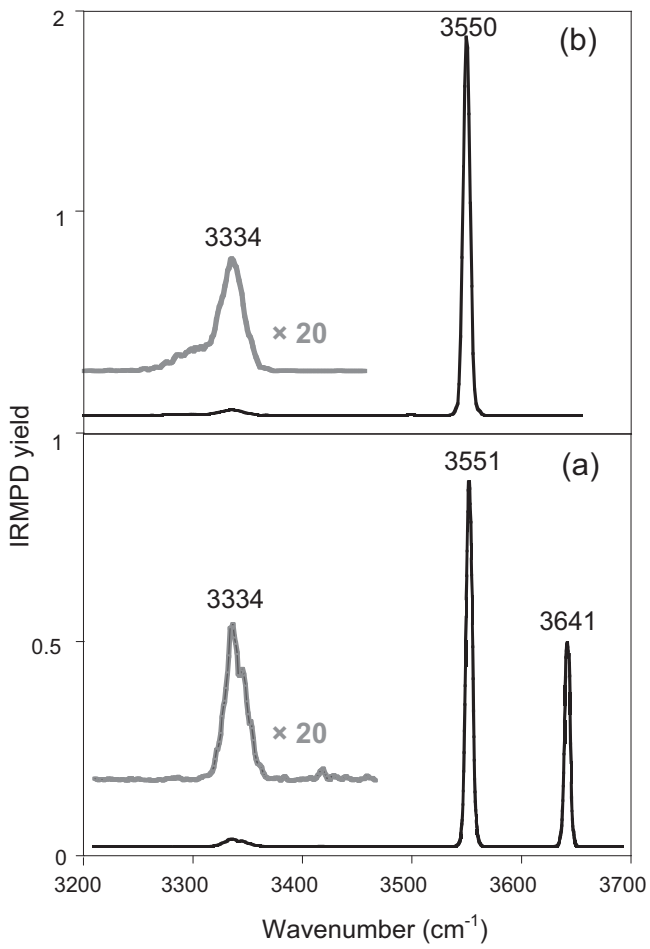

Fig. 7. IRMPD spectrum of $[Tyr+H]^+$ (a) and of $[nitroTyr+H]^+$ (b) in the N–H and O–H stretching vibration region.

are reported in Fig. 8S in the Supplementary Data together with the experimental spectrum, while band positions and mode assignments are summarized in Table 2. The sharp feature at 3550 cm^{-1} (fwhm = 6 cm^{-1}) in the spectrum of $[nitroTyr+H]^+$ is associated to the free OH stretching of the carboxylic group calculated at 3551 cm^{-1}. The calculated spectrum shows the OH stretching mode of the ring hydroxyl group at 3332 cm^{-1} while the NH stretching vibration involving the hydrogen atom that is free from either H-bonding to the carbonyl group or interaction with the π system is expected at 3319 cm^{-1}. Notably, the ring hydroxyl group interacts by hydrogen bonding with the ortho nitro group. In the absence of this strong interaction, the ring OH stretching of protonated tyrosine has been recorded at 3641 cm^{-1} (Fig. 7a). The conformer mixture (**2a–d**) accounting for protonated unsubstituted tyrosine has been characterized in detail by conformer-specific IR depletion spectroscopy in the wavelength range of 3000–3700 cm^{-1} [49] and the calculated IR spectra are illustrated in Fig. 9S. Fig. 7b shows

Table 2
IRMPD spectral frequencies of protonated 3-nitrotyrosine $[nitroTyr+H]^+$, and calculated (B3LYP/6-311++G**) vibrational frequencies of conformer **1a**.

Experimental IRMPD[a]	Calculated IR[a,b]	Vibrational mode
1171	1163 (274)	C–O stretch and COH bend of C(O)OH
	1179 (87)	C–H and COH bend of aryl group, ring def
	1209 (64)	C–H and COH bend of aryl group, ring def
1273	1271 (145)	symm NO_2 stretch, CH bend, ring def
	1292 (170)	C–NO_2 stretch, CH and COH bend of aryl group
1329	1347 (107)	symm NO_2 stretch, aryl C–OH stretch, side chain C–H bend
	1376 (65)	CH and COH bend of aryl group, ring def
	1391 (102)	CCO stretch of side chain, CH bend of side chain methine
1421	1444 (199)	NH_3 umbrella
1473	1489 (107)	asymm NO_2 stretch, C=C and C–O stretch, aromatic CH bend
1540	1555 (212)	asymm NO_2 stretch, C=C stretch, aromatic CH bend
1614	1629 (190)	NH_2 scissor, C=C stretch
1757	1766 (288)	C=O stretch
	3200 (361)	asymm NH_2 stretch (H's bound to CO and to aromatic system)
3334	3319 (127)	NH stretch (free)
	3332 (273)	OH stretch (ring)
3550	3551 (209)	OH stretch of C(O)OH

[a] In cm^{-1}.
[b] Only major bands (intensity greater than 50 km mol^{-1}, reported in parentheses) are listed.

also a distinct feature at 3334 cm^{-1}, though somewhat broader and weaker than expected on the basis of the calculated IR spectrum of $[nitroTyr + H]^+$, which might be assigned to the unresolved ring OH stretching and free NH stretching modes. However, hydrogen bonding is known to cause both a red-shift and a pronounced broadening effect of OH and NH stretching vibrations to the point of rendering their identification difficult. This effect has been observed for example in water solvated ammonium clusters and in hydrated, protonated aminoacids and nucleobases [58–61]. It is therefore likely that the band at 3334 cm^{-1} be due to the activity of the free NH stretch. The stretching vibrations associated to the remaining two NH bonds, where the H atom is either engaged as hydrogen bond donor to the carbonyl group or is interacting with the π system, are calculated at 3200 cm^{-1} (asymm) and at 3140 cm^{-1} (symm, very weak). These modes are red shifted with respect to the former and are expected to show pronounced anharmonicity [49]. It is probably for these reasons that they do not yield any signal above baseline noise.

Overall, IRMPD spectroscopy appears less interesting in the 3000–3700 cm^{-1} range if one aims at revealing characteristic nitration signatures. In fact, the remarkable difference between the IRMPD spectrum of $[nitroTyr + H]^+$ and the one of $[Tyr + H]^+$ is rather the missing band of the free OH stretching mode associated to the ring hydroxyl substituent while there is not any additional peculiar feature.

4. Conclusions

The protonated 3-nitrotyrosine ion $[nitroTyr + H]^+$, has been studied by an approach based on tandem mass spectrometry and IR 'action' spectroscopy aimed at characterizing an important post-translational modification and a potential marker for pathological states. IRMPD spectroscopy in the 1000–2000 cm^{-1} range has provided a clear indication of diagnostic bands associated to the presence of the nitro group. To this end, the comparison of the IRMPD spectra of $[nitroTyr + H]^+$ and of $[Tyr + H]^+$ is revealing. The dominant band at 1329 cm^{-1} in the IRMPD spectrum of $[nitroTyr + H]^+$, assigned to the aryl C–OH stretching and symmetric NO_2 stretching, is missing in the spectrum of $[Tyr + H]^+$. A second characteristic, though less intense, band is observed at 1540 cm^{-1} and is ascribed to a major contribution of asymmetric NO_2 stretching. The remaining IR features present in the IRMPD spectrum of $[nitroTyr + H]^+$ match nicely with the corresponding ones belonging to $[Tyr + H]^+$. While it is by no means surprising to note additional bands associated to vibrations of the nitro groups, the intensity of the band at 1329 cm^{-1} is remarkable. The IR spectrum calculated at B3LYP/6-311++G** level does not account for such a high activity. Tentative reasons may stem from a failure of the adopted DFT calculations to provide an accurate description of the IR spectrum or to the operation of effects attached to the multiple photon nature of IRMPD spectroscopy [21,55–62]. It is, however, a favorable event that a prominent feature allows a clear distinction between the native $[Tyr + H]^+$ and the modified $[nitroTyr + H]^+$ species. Ultimately, the photolability of nitrotyrosine, a drawback affecting MALDI analysis, may hopefully be turned into a diagnostic assay.

Acknowledgements

Financial support was provided by the Italian Ministero dell'Istruzione, dell'Università e della Ricerca and by the European Community's Seventh Framework Programme (FP7/2007-2013, under grant agreement n° 226716) which provided also travel funding to M. E. C. and B. C. for access to the European multi-user facility CLIO. The skilful assistance of the CLIO team is gratefully acknowledged.

Appendix A. Supplementary data

Supplementary data associated with this article can be found, in the online version, at doi:10.1016/j.ijms.2011.07.012.

References

[1] R. Radi, Nitric oxide, oxidants, and protein tyrosine nitration, Proc. Natl. Acad. Sci. U.S.A. 101 (2004) 4003–4008.
[2] H. Rubbo, R. Radi, Protein and lipid nitration: role in redox signaling and injury, Biochim. Biophys. Acta 1780 (2008) 1318–1324.
[3] J.M. Souza, G. Peluffo, R. Radi, Protein tyrosine nitration-functional alteration or just a biomarker? Free Radic. Biol. Med. 45 (2008) 357–366.
[4] J.S. Beckman, Oxidative damage and tyrosine nitration from peroxynitrite, Chem. Res. Toxicol. 9 (1996) 836–844.
[5] A. Amoresano, G. Chiappetta, P. Pucci, M. D'Ischia, G. Marino, Bidimensional tandem mass spectrometry for selective identification of nitration sites in proteins, Anal. Chem. 79 (2007) 2109–2117.
[6] N. Abello, H.A.M. Kerstjens, D.S. Postma, R.J. Bischoff, Protein tyrosine nitration: selectivity, physicochemical, and biological consequences, denitration, and proteomics methods for the identification of tyrosine nitrated proteins, Proteome Res. 8 (2009) 3222–3238.
[7] I. Dalle-Donne, A. Scaloni, D. Giustarini, E. Cavarra, G. Tell, G. Lungarella, R. Colombo, R. Rossi, A. Milzani, Proteins as biomarkers of oxidative/nitrosative stress in diseases: the contribution of redox proteomics, Mass Spectrom. Rev. 24 (2005) 55–99.
[8] P. Schmidt, N. Youhnovski, A. Daiber, A. Balan, M. Arsic, M. Bachschmid, M. Przybylski, V. Ullrich, Specific nitration at tyrosine 430 revealed by high resolution mass spectrometry as basis for redox regulation of bovine prostacyclin synthase, J. Biol. Chem. 278 (2003) 12813–12819.
[9] M. Ulrich, A. Petre, N. Youhnovski, F. Proemm, M. Schirle, M. Schumm, R.S. Pero, A. Doyle, J. Checkel, H. Kita, N. Thiyagarajan, K.R. Acharya, P. Schmid-Grendelmeier, H.-U. Simon, H. Schwarz, M. Tsutsui, H. Shimokawa, G. Bellon, J.J. Lee, M. Przybylski, G. Doering, Post-translational tyrosine nitration of eosinophil granule toxins mediated by eosinophil peroxidase, J. Biol. Chem. 283 (2008) 28629–28640.
[10] B.-A. Petre, N. Youhnovski, J. Lukkari, R. Weber, M. Przybylski, Structural characterisation of tyrosine-nitrated peptides by ultraviolet and infrared matrix-assisted laser desorption/ionisation Fourier transform ion cyclotron resonance mass spectrometry, Eur. J. Mass Spectrom. 11 (2005) 513–518.
[11] A.W. Jones, V.A. Mikhailov, J. Iniesta, H.J. Cooper, Electron capture dissociation mass spectrometry of tyrosine nitrated peptides, J. Am. Soc. Mass Spectrom. 21 (2010) 268–277.
[12] A.S. Petersson, H. Steen, D.E. Kalume, K. Caidahl, P. Roepstorff, Investigation of tyrosine nitration in proteins by mass spectrometry, J. Mass Spectrom. 36 (2001) 616–625.
[13] A. Sarver, N.K. Scheffler, M.D. Shetlar, B.W. Gibson, Analysis of peptides and proteins containing nitrotyrosine by matrix-assisted laser desorption/ionization mass spectrometry, J. Am. Soc. Mass Spectrom. 12 (2001) 439–448.
[14] B. Ghesquière, M. Goethals, J. Van Damme, A. Staes, E. Timmerman, J. Vandekerckhove, K. Gevaert, Improved tandem mass spectrometric characterization of 3-nitrotyrosine sites in peptides, Rapid Commun. Mass Spectrom. 20 (2006) 2885–2893.
[15] I.V. Turko, F. Murad, Mapping sites of tyrosine nitration by matrix-assisted laser desorption/ionization mass spectrometry, Methods Enzymol. 396 (2005) 266–275.
[16] X. Zhan, D.M. Desiderio, Linear ion-trap mass spectrometric characterization of human pituitary nitrotyrosine-containing proteins, Int. J. Mass Spectrom. 259 (2007) 96–104.
[17] J.R. Eyler, Infrared multiple photon dissociation spectroscopy of ions in penning traps, Mass Spectrom. Rev. 28 (2009) 448–467.
[18] T.D. Fridgen, Infrared consequence spectroscopy of gaseous protonated and metal ion cationized complexes, Mass Spectrom. Rev. 28 (2009) 586–607.
[19] N.C. Polfer, J. Oomens, Vibrational spectroscopy of bare and solvated ionic complexes of biological relevance, Mass Spectrom. Rev. 28 (2009) 468–494.
[20] L. MacAleese, P. Maitre, Infrared spectroscopy of organometallic ions in the gas phase: from model to real world complexes, Mass Spectrom. Rev. 26 (2007) 583–605.
[21] J. Oomens, B.G. Sartakov, G. Meijer, G. von Helden, Gert, Gas-phase infrared multiple photon dissociation spectroscopy of mass-selected molecular ions, Int. J. Mass Spectrom. 254 (2006) 1–19.
[22] C. Kapota, J. Lemaire, P. Maitre, G. Ohanessian, Vibrational signature of charge solvation vs salt bridge isomers of sodiated amino acids in the gas phase, J. Am. Chem. Soc. 126 (2004) 1836–1842.
[23] N.C. Polfer, B. Paizs, L.C. Snoek, I. Compagnon, S. Suhai, G. Meijer, G. Von Helden, J. Oomens, Infrared fingerprint spectroscopy and theoretical studies of potassium ion tagged amino acids and peptides in the gas phase, J. Am. Chem. Soc. 127 (2005) 8571–8579.
[24] N.C. Polfer, J. Oomens, R.C. Dunbar, IRMPD spectroscopy of metal-ion/tryptophan complexes, Phys. Chem. Chem. Phys. 8 (2006) 2744–2751.

[25] P.B. Armentrout, M.T. Rodgers, J. Oomens, J.D. Steill, Infrared multiphoton dissociation spectroscopy of cationized serine: effects of alkali-metal cation size on gas-phase conformation, J. Phys. Chem. A 112 (2008) 2248–2257.
[26] M.T. Rodgers, P.B. Armentrout, J. Oomens, J.D. Steill, Infrared multiphoton dissociation spectroscopy of cationized threonine: effects of alkali-metal cation size on gas-phase conformation, J. Phys. Chem. A 112 (2008) 2258–2267.
[27] M.W. Forbes, M.F. Bush, N.C. Polfer, J. Oomens, R.C. Dunbar, E.R. Williams, R.A. Jockusch, Infrared spectroscopy of arginine cation complexes: direct observation of gas-phase zwitterions, J. Phys. Chem. A 111 (2007) 11759–11770.
[28] M.F. Bush, J.T. O'Brien, J.S. Prell, R.J. Saykally, E.R. Williams, Infrared spectroscopy of cationized arginine in the gas phase: direct evidence for the transition from nonzwitterionic to zwitterionic structure, J. Am. Chem. Soc. 129 (2007) 1612–1622.
[29] M.F. Bush, M.W. Forbes, R.A. Jockusch, J. Oomens, N.C. Polfer, R.J. Saykally, E.R. Williams, Infrared spectroscopy of cationized lysine and ε-N-methyllysine in the gas phase: effects of alkali-metal ion size and proton affinity on zwitterion stability, J. Phys. Chem. A 111 (2007) 7753–7760.
[30] M. Citir, E.M.S. Stennett, J. Oomens, J.D. Steill, M.T. Rodgers, P.B. Armentrout, Infrared multiple photon dissociation spectroscopy of cationized cysteine: effects of metal cation size on gas-phase conformation, Int. J. Mass Spectrom. 297 (2010) 9–17.
[31] M.K. Drayss, P.B. Armentrout, J. Oomens, M. Schäfer, IR spectroscopy of cationized aliphatic amino acids: stability of charge-solvated structure increases with metal cation size, Int. J. Mass Spectrom. 297 (2010) 18–27.
[32] J.M. Bakker, T. Besson, J. Lemaire, D. Scuderi, P. Maître, Gas-phase structure of a π-allyl–palladium complex: efficient infrared spectroscopy in a 7T Fourier transform mass spectrometer, J. Phys. Chem. A 111 (2007) 13415–13424.
[33] J.J. Valle, J. Eyler, J. Oomens, D.T. Moore, A.F.G. van der Meer, G. von Helden, G. Meijer, C. Hendrickson, A.G. Marshall, G.T. Blakney, Free electron laser-Fourier transform ion cyclotron resonance mass spectrometry facility for obtaining infrared multiphoton dissociation spectra of gaseous ions, Rev. Sci. Instrum. 76 (2005) 023103/1–123103/.
[34] P. Maitre, S. Le Caër, A. Simon, W. Jones, J. Lemaire, H. Mestdagh, M. Heninger, G. Mauclaire, P. Boissel, R. Prazeres, F. Glotin, J.-M. Ortega, Ultrasensitive spectroscopy of ionic reactive intermediates in the gas phase performed with the first coupling of an IR FEL with an FTICR-MS, Nucl. Instrum. Methods Phys. Res. A 507 (2003) 541–546.
[35] R.K. Sinha, P. Maître, S. Piccirillo, B. Chiavarino, M.E. Crestoni, S. Fornarini, Cysteine radical cation: a distonic structure probed by gas phase IR spectroscopy, Phys. Chem. Chem. Phys. 12 (2010) 9794–9800.
[36] P. Maitre, J. Lemaire, D. Scuderi, Structural characterization under tandem mass spectrometry conditions: infrared spectroscopy of gas phase ions, Phys. Scr. 78 (2008) 058111/1–058111/6.
[37] C.F. Correia, P.O. Balaj, D. Scuderi, P. Maitre, G. Ohanessian, Vibrational signatures of protonated, phosphorylated amino acids in the gas phase, J. Am. Chem. Soc. 130 (2008) 3359–3370.
[38] C.F. Correia, C. Clavaguera, U. Erlekam, D. Scuderi, G. Ohanessian, IRMPD Spectroscopy of a protonated, phosphorylated dipeptide, ChemPhysChem 9 (2008) 2564–2573.
[39] M. Ignasiak, D. Scuderi, P. de Oliveira, T. Pedzinski, Y. Rayah, C. Houee Levin, Characterization by mass spectrometry and IRMPD spectroscopy of the sulfoxide group in oxidized methionine and related compounds, Chem. Phys. Lett. 502 (2011) 29–36.
[40] J. Lemaire, P. Boissel, M. Heninger, G. Mauclaire, G. Bellec, H. Mestdagh, A. Simon, S. Le Caer, J.M. Ortega, F. Glotin, P. Maitre, Gas phase infrared spectroscopy of selectively prepared ions, Phys. Rev. Lett. 89 (2002) 273002–273004.
[41] J.S. Prell, J.T. O'Brien, E.R. Williams, IRPD spectroscopy and ensemble measurements: effects of different data acquisition and analysis methods, J. Am. Soc. Mass Spectrom. 21 (2010) 800–809.
[42] S. Gronert, D.C. Simpson, K.M. Conner, A reevaluation of computed proton affinities for the common α-amino acids, J. Am. Soc. Mass Spectrom. 20 (2009) 2116–2123.
[43] G. Bouchoux, S. Bourcier, V. Blanc, S. Desaphy, Gas phase protonation thermochemistry of phenylalanine and tyrosine, J. Phys. Chem. B 113 (2009) 5549–5562.
[44] Z.B. Maksic, B. Kovacevic, Towards the absolute proton affinities of 20 α-amino acids, Chem. Phys. Lett. 307 (1999) 497–504.
[45] T.C. Dinadayalane, G.N. Sastry, J. Leszczynski, Comprehensive theoretical study towards the accurate proton affinity values of naturally occurring amino acids, Int. J. Quant. Chem. 106 (2006) 2920–2933.
[46] H. Lioe, R.J. O'Hair, Comparison of collision-induced dissociation and electron-induced dissociation of singly protonated aromatic amino acids, cystine and related simple peptides using a hybrid linear ion trap-FT-ICR mass spectrometer, Anal. Bioanal. Chem. 389 (2007) 1429–1437.
[47] H. El Aribi, G. Orlova, A.C. Hopkinson, K.W.M. Siu, Gas-phase fragmentation reactions of protonated aromatic amino acids: concomitant and consecutive neutral eliminations and radical cation formations, J. Phys. Chem. A 108 (2004) 3844–3853.
[48] F. Rogalewicz, Y. Hoppilliard, G. Ohanessian, Fragmentation mechanisms of α-amino acids protonated under electrospray ionization: a collisional activation and ab initio theoretical study, Int. J. Mass Spectrom. 195/196 (2000) 565–590.
[49] J.A. Stearns, S. Mercier, C. Seaiby, M. Guidi, O.V. Boyarkin, T.R. Rizzo, Conformation-specific spectroscopy and photodissociation of cold, protonated tyrosine and phenylalanine, J. Am. Chem. Soc. 129 (2007) 11814–11820.
[50] H. Kang, C. Jouvet, C. Dedonder-Lardeux, S. Martrenchard, G. Gregoire, G. Desfrancois, J.-P. Schermann, M. Barat, J.A. Fayeton, Ultrafast deactivation mechanisms of protonated aromatic amino acids following UV excitation, Phys. Chem. Chem. Phys. 7 (2005) 394–398.
[51] C. Bleiholder, S. Suhai, B. Paizs, Revising the proton affinity scale of the naturally occurring α -amino acids, J. Am. Soc. Mass Spectrom. 17 (2006) 1275–1281.
[52] A.G. Harrison, The gas-phase basicities and proton affinities of amino acids and peptides, Mass Spectrom. Rev. 16 (1997) 201–217.
[53] R. Wu, T.B. McMahon, Investigation of cation-π interactions in biological systems, J. Am. Chem. Soc. 130 (2008) 12554–12555.
[54] R. Wu, T.B. McMahon, An investigation of protonation sites and conformations of protonated amino acids by IRMPD spectroscopy, ChemPhysChem 9 (2008) 2826–2835.
[55] D. Schröder, H. Schwarz, P. Milko, J. Roithová, Dissociation routes of protonated toluene probed by infrared spectroscopy in the gas phase, J. Phys. Chem. A 110 (2006) 8346–8353.
[56] D.T. Moore, J. Oomens, J.R. Eyler, G. von Helden, G. Meijer, R.C. Dunbar, Infrared spectroscopy of gas-phase Cr^+ coordination complexes: determination of binding sites and electronic states, J. Am. Chem. Soc. 129 (2005) 7243–7254.
[57] R.K. Sinha, B. Chiavarino, S. Fornarini, J. Lemaire, P. Maitre, M.E. Crestoni, Protonated sulfuric acid: vibrational signatures of the naked ion in the near- and mid-IR, J. Phys. Chem. Lett. 1 (2010) 1721–1724.
[58] J.M. Bakker, J.-Y. Salpin, P. Maitre, Tautomerism of cytosine probed by gas phase IR spectroscopy, Int. J. Mass Spectrom. 283 (2009) 214–221.
[59] J.M. Bakker, R.K. Sinha, T. Besson, M. Brugnara, P. Tosi, J.-Y. Salpin, P. Maitre, Tautomerism of uracil probed via infrared spectroscopy of singly hydrated protonated uracil, J. Phys. Chem. A 112 (2008) 12393–12400.
[60] A. Kamariotis, O.V. Boyarkin, S.R. Mercier, R.D. Beck, M.F. Bush, E.R. Williams, T.R. Rizzo, Infrared spectroscopy of hydrated amino acids in the gas phase: protonated and lithiated valine, J. Am. Chem. Soc. 128 (2006) 905–916.
[61] Y.-S. Wang, H.-C. Chang, J.-C. Jiang, S.H. Lin, Y.T. Lee, H.-C. Chang, Structures and isomeric transitions of $NH_4^+(H_2O)_{3-6}$: from single to double rings, J. Am. Chem. Soc. 120 (1998) 8777–8788.
[62] J.S. Prell, T.M. Chang, J.A. Biles, G. Berden, J. Oomens, E.R. Williams, Isomer population analysis of gaseous ions from infrared multiple photon dissociation kinetics, J. Phys. Chem. A 115 (2011) 2745–2751.